A Look At Three Different Scenarios for Bulge Formation

Rychard Bouwens

Physics Department, University of California, Berkeley, CA 94720;
bouwens@astro.berkeley.edu

&

Laura Cayón

Instituto de Física de Cantabria, CSIC-Universidad de Cantabria, 39005 Santander
(Cantabria), Spain; cayon@ifca.unican.es

&

Joseph Silk

Astronomy and Physics Departments, and Center for Particle Astrophysics, University of
California, Berkeley, CA 94720; silk@astro.berkeley.edu

ABSTRACT

In this paper, we present three qualitatively different scenarios for bulge formation: a secular evolution model in which bulges form after disks and undergo several central starbursts, a primordial collapse model in which bulges and disks form simultaneously, and an early bulge formation model in which bulges form prior to disks. We normalize our models to the local $z = 0$ observations of de Jong & van der Kruit (1994) and Peletier & Balcells (1996) and make comparisons with high redshift observations. We consider model predictions relating directly to bulge-to-disk properties. As expected, smaller bulge-to-disk ratios and bluer bulge colors are predicted by the secular evolution model at all redshifts, although uncertainties in the data are currently too large to differentiate strongly between the models.

Subject headings: galaxies: evolution

1. Introduction

A number of different mechanisms have been proposed for the formation of bulges: primordial collapse (Eggen, Lynden-Bell, & Sandage 1962), hierarchical galaxy formation

models (Kauffmann & White 1993, Baugh et al. 1996), infall of satellite galaxies, and the secular evolution of galaxy disks. Numerous arguments have been put forward that secular evolution of disks has occurred in at least some galaxies, particularly in late-type galaxies (Kormendy 1992; Courteau 1996). However, for some galaxies, notably those with a massive bulge, simple energy arguments show that not all galaxies could have formed in this way. Such galaxies would have necessarily formed by primordial collapse, major mergers at high redshifts, or infall of satellite galaxies (Pfenniger 1992). In summary, it appears that many mechanisms have been at work in forming bulges over the history of universe, and so the question is no longer which mechanisms were effective in forming bulges but in what fraction.

In this paper, we shall broadly classify these bulge formation scenarios into three types: secular evolution in which bulges form relatively late by a series of bar-induced starbursts, one in which bulges form simultaneously with disks, and an early bulge formation model in which bulges form earlier than disks. Adjusting the three models to produce optimal agreement with $z = 0$ observations, we compare their high-redshift predictions with present observations, in particular, with data compiled in various studies based on the CFRS (Schade et al. 1995; Schade et al. 1996; Lilly et al. 1998) and the HDF (Abraham et al. 1998).

We begin by presenting the samples used to constrain the models (§2), follow with a description of the models (§3), provide a brief description of our computational method (§4), move onto our high-redshift predictions and comparisons with available observations (§5), and finally summarize the implications of our analysis (§6). Hereinafter, we use $H_o = 50$ km/s/Mpc.

2. Local $z = 0$ Samples

For the purposes of normalizing our models, we examine two local $z = 0$ samples: the de Jong sample (de Jong & van der Kruit 1994; de Jong 1995, 1996; hereinafter, DJ) and the Peletier & Balcells sample of galaxies (Peletier et al. 1994; Peletier & Balcells 1996; hereinafter, PB). The DJ sample is selected from $\sim 12.5\%$ of the sky and considers only relatively face-on ($b > 0.625$) galaxies (37.5% of all orientations). For simplicity, we shall treat selection of this sample to be on $\sim 4.7\%$ of the sky (*e.g.,* 0.59 steradians). Following de Jong (1996), we also take it to be diameter-limited in R to galaxies larger than 2′ at 24.7 R-mag arcsec^2.

The PB sample is a similarly diameter-limited sample: the B-band diameter in terms

of its 25 mag/arcsec^2 isophote was restricted to the range $90''$ and $150''$. However, in contrast to the relatively face-on ($b > 0.625$) DJ sample, the PB sample considers galaxies of all orientations, and this was our principal reason for including it in our comparisons. Unfortunately, the PB sample is more restricted than the DJ sample in the Hubble types included (3.0 to 6.5) and in the surface brightness range ($20.5 < \mu_0^{b_J} < 21.5$).

In the model comparisons which follow, we select our local $z = 0$ subsample from the local samples using the DJ selection criteria since the PB sample is roughly a subset of the DJ sample strictly in terms of the selection criteria. We attempt to normalize the PB sample relative to the DJ sample so that it contains 31% of the number in the de Jong sample since ~ 752 out of 1207 galaxies (62%) in the ESO-LF catalogue down to $1'$ (Lauberts & Valentijn 1989) were of type 3.0 to 6.5 (Sbcd) and roughly 50% of the DJ sample was in the PB surface brightness selection range. In principle, then, the PB sample should be a simple subset of the DJ sample. Unfortunately, a simple look at the relative colour and B/T distributions for the DJ and PB samples indicates that there are more galaxies in the PB sample with large B/T ratios and relatively blue bulges than in the DJ sample. Many of these differences can be attributed to the fact that the properties of the DJ sample were measured from face-on galaxies while the PB sample covered a range of inclination angles. Edge-on disks in the PB sample are simply redder and less prominent relative to the bulges due to the greater path length the light must traverse through the dusty disks.

In all of the model comparisons which follow, due to the various complications associated with the exact meaning of UGC R diameter, the relative fraction of low surface brightness galaxies, and the influence of disk orientation on selection, we simply adjust the surface brightness threshold at which the UGC diameters (from which the DJ sample was taken) were measured to obtain rough agreement with the number of galaxies obtained in the DJ sample.

3. Models

Starting with the local properties of disks and a reasonable distribution of formation times, we construct a fiducial disk evolution model, to which we add three different models for bulge formation, the principle difference being simply the time the bulges form relative to that of their associated disks. Since it is simply our intent to examine the extent to which current observations allow us to discriminate the order in which bulges and disks form, we intentionally do not consider a more complex model (e.g., Kauffmann et al. 1993; Baugh et al. 1996; Molla & Ferrini 1995) nor do we attempt to model the internal dynamics

or structure of spirals (e.g., Friedli & Benz 1995).

We assume the Sabc and Sdm luminosity functions (LFs) for disk galaxies given by Binggeli, Sandage, and Tammann (1988). We adjust the bulge-to-total (B/T) distributions of these galaxy types to obtain fair agreement with those distributions measured in the DJ and PB samples (see Figure 3). We evolve these galaxies backwards in time in luminosity according to their individual star formation histories without number evolution, presuming that significant evolution in number occurs only at redshifts above those examined in the present study ($0 < z < 1$). For this reason, we do not make predictions above $z \sim 1$.

We take the formation times of these galaxies to be distributed identically to that given by the procedure outlined in Section 2.5.2 of Lacey & Cole (1993) except that we take halo formation time to equal the time over which 0.25 of the final halo mass is assembled. For the purposes of calculating halo formation times corresponding to galaxies of a given luminosity, we assume a constant mass-to-light ratio where a $M_{b_J} = -21.1$ galaxy has $4 \cdot 10^{12} M_\odot$ and we adopt the CDM matter power spectrum given in White & Frenk (1991):

$$P(k) = \frac{1.94 \times 10^4 b^{-2} k}{(1 + 6.8k + 72k^{3/2} + 16k^2)^2} \mathrm{Mpc}^3 \tag{1}$$

For $b = 1$, this expression yields $\sigma_8 = 1$.

Just as we choose to take the halo formation time to be the time over which 0.25 of the final halo mass is assembled instead of 0.5 used by Lacey & Cole (1993), we choose $\Omega = 0.15$ to push the epoch of large-scale merging to high enough redshift so that the observed number of stars are able to build up in these galaxies without being destroyed by the merging events prevalent at earlier epochs. Since we have observable constraints on the star formation history of the universe, there is a certain epoch after which disks must remain largely undisturbed. Of course, if we had assumed that some fraction of the stars in the disk were added by minor mergers, we could push the halo formation time, and consequently the formation of disks and bulges, to lower redshift by raising the value of Ω. We illustrate the distribution of halo formation times in Figure 1 for several different luminosity ranges.

We take star formation in the disk to commence at the halo formation time with an e-folding time that depends on the $z = 0$ galaxy luminosity, i.e., $\tau = (3\,\mathrm{Gyr})10^{0.4(M_{b_J}+20)}$ to roughly fit the $z = 0$ colour-magnitude relationship (see Figure 2), so that the star formation rate in the disk of a galaxy with absolute magnitude M_{b_J} and halo formation time t_{HF} can be expressed:

$$SFR_{disk} \propto \begin{cases} e^{-(t_{HF}-t)/\tau} & t < t_{HF}, \\ 0 & t \geq t_{HF}. \end{cases} \tag{2}$$

We adopt the standard equations for evolution in metallicity to $z = 0$ (Tinsley 1980) and tune the yields for each luminosity separately to reproduce the $z = 0$ disk metallicities given by $[Fe/H] = (-0.17)(M_Z + 20) - 0.28$ (Zaritsky, Kennicutt, & Huchra 1994). Since we are not trying to develop a universal model for chemical evolution in disks, we have simply tuned the yields for each luminosity separately.

Using the Calzetti (1997) extinction prescription and a screen model for the dust, we take the optical depth τ of dust in the B band to equal $0.7(10^{-0.17(1.3)(M_B+19.72)})$, consistent with the values given in Peletier et al. (1995). We assume exponential profiles for the disks with a b_J central surface brightness given by $21.65 + 0.2(M_B + 21)$ for simplicity where this expression accounts for the observed correlation between surface brightness and luminosity (e.g., de Jong 1996; McGaugh & de Blok 1997). We compute spectra for the purposes of determining colours and magnitudes using the Bruzual & Charlot instantaneous-burst metallicity-dependent spectral synthesis tables as compiled in Leitherer et al. (1996). For metallicities in between those compiled here, we have interpolated between the provided tables in units of $\log Z$.

To calibrate our fiducial disk evolution models, we compare the model predictions to both the colour-magnitude relationship of disks in spirals and the cosmic history of luminosity density. Firstly, with regard to the colour-magnitude relationship, we note that we produce good agreement with the colour-magnitude relationship given in the DJ and PB samples, both in terms of their slopes and overall distributions (Figure 2). Given our relatively reasonable assumptions about the quantity of dust and metals in these galaxies, matching these distributions gives us a basic constraint on the star formation history in disk galaxies of different luminosities. Secondly, all models, for which bulge, disk, and E/S0 contributions have been considered, produce fair agreement with the luminosity density of the universe at all redshifts for which observable constraints are available (Lilly et al. 1996; Madau et al. 1996; Connolly et al. 1997), though the observed luminosity density is slightly lower at lower redshifts (Figure 3). Resolving this discrepancy requires pushing the formation of disk galaxies to higher redshifts, i.e., lowering Ω. Discrepancies in the ultraviolet luminosity density could be easily removed by introducing moderate dust extinction at high z, as motivated by many recent analyses (Sawicki & Yee 1998; Calzetti 1997; Meurer et al. 1997). Note that the similarities of the models at high redshift follows from the dominant and identical E/S0 contribution. Having described our fiducial disk model, we now describe the basic three models for bulge formation that we will be comparing.

Secular Evolution Model: In the secular evolution scenario, bulges form after disks. In this scenario, gas accretion onto the disk triggers the formation of a bar, gas-inflow into

the center, and then star formation in the galaxy center (Friedli & Benz 1995; Norman, Sellwood, & Hasan 1996). The build-up of a central mass destroys the bar and inhibits gas inflow, consequently stopping star formation in the bulge until enough gas accretes onto the galaxy to trigger the formation of a second bar, gas inflow into the center, and finally a second central starburst. Somewhat arbitrarily, we suppose that the first central starburst occurs some 2 Gyr after disk formation in our fiducial model, that central starbursts last 0.1 Gyr, a time-scale matching those found in the detailed simulations by Friedli & Benz (1995), and that 2.4 Gyr separates central starbursts, numbers used just to illustrate the general effect of a late secular evolution model for the bulge. We repeat this cycle indefinitely and assume that the star formation rate follows an envelope with an e-folding time equivalent to the history of disk star formation:

$$SFR_{bulge} \propto \begin{cases} e^{-(t_{HF}-2Gyr-t)/\tau} & \frac{t_{HF}-2Gyr-t}{2.5Gyr} - \lfloor \frac{t_{HF}-2Gyr-t}{2.5Gyr} \rfloor < 0.04, \\ 0 & \frac{t_{HF}-2Gyr-t}{2.5Gyr} - \lfloor \frac{t_{HF}-2Gyr-t}{2.5Gyr} \rfloor \geq 0.04, \\ 0 & t \geq t_{HF} - 2Gyr \end{cases} \quad (3)$$

where $\lfloor \ \rfloor$ is the greatest integer function. We thereby force star formation in the disk and the bulge to follow very similar time scales, given the extent to which they are both driven by gas infall processes. Of course, bulge growth over the history of the universe should affect these time-scales, but given the already large uncertainties in both gas accretion and star formation, we have decided to ignore this. For all bulge models, we adopt the slope of the approximate luminosity-metallicity relationship $[Fe/H] = -(0.02/0.135)M_R - 3.1852$ (González & Gorgas 1996; Jablonka et al. 1996; Buzzoni et al. 1992). For the secular evolution model we fix the metallicity at the $z = 0$ value somewhat crudely to account for the fact that this gas would already be polluted by stars which formed in the disk.

Simultaneous Formation Model: We assume for our second model that star formation in the bulge commences at the formation time of disks in our fiducial model. In this model, high angular momentum gas forms the disk while the low angular momentum gas simultaneously forms the bulge. As in the secular evolution model, we suppose that the star formation in the bulge lasts $\tau_{burst} = 0.1$ Gyr so that

$$SFR_{bulge} \propto \begin{cases} e^{-(t_{HF}-t)/\tau_{burst}} & t < t_{HF}, \\ 0 & t \geq t_{HF}. \end{cases} \quad (4)$$

To obtain distributions of bulge colours for both the simultaneous and the early bulge formation models that match the data, we systematically decrease the metallicity of bulges by 0.2 relative to the relationship preferred by Jablonka et al. (1996). As in the disk, we assume evolution in the metallicity of the gas that forms the bulge.

Early Bulge Formation Model: In models where bulges form through the merging of disk galaxies, the formation of the stars found in bulges is expected to precede the formation

of stars in the disks which form out of gas which accretes around the spheroid (e.g., Kauffmann & White 1993; Frenk et al. 1996). For simplicity, we commence star formation in the bulge 4 Gyr prior to the formation of disks in our fiducial model and suppose that it lasts $\tau_{burst} = 0.1$ Gyr as in our other models so that

$$SFR_{bulge} \propto \begin{cases} e^{-(t_{HF}+4Gyr-t)/\tau_{burst}} & t < t_{HF} + 4Gyr, \\ 0 & t \geq t_{HF} + 4Gyr. \end{cases} \tag{5}$$

Finally, to these models, we add a simple model for E/S0 galaxies to aid with the interpretation of observed high redshift, high B/T systems. We adopt the same luminosity function for the E/S0 galaxies given in Pozzetti et al. (1996) but with a 20% higher normalization to somewhat better fit the observed evolution in luminosity densities. We somewhat arbitrarily assume that the distribution of formation redshifts for the $E/S0$ population is scaled to be at exactly twice the distribution of formation redshifts obtained for the same luminosity spiral in the b_J band so that if the median formation redshift for some luminosity spiral is 1, the median formation redshift for the same luminosity E/S0 is 2. We take the e-folding time for star formation to be 0.5 Gyr. Since it is likely that the stars in ellipticals were assembled from other galactic fragments through mergers, this scenario is only intended to be representative of when the stars in elliptical galaxies formed rather than where they formed. We assume that the $E/S0$ population has B/T ratios distributed between 0.5 and 1 with a scatter intended to represent both the intrinsic uncertainty in the relative local mix of E and $S0$ galaxies and the realistic scatter in B/T values extracted in typical bulge-to-total luminosity decompositions (*e.g.*, Ratnatunga et al. 1998). We further assume that the metallicity of all the stars in our E/S0 population are of solar metallicity.

4.   Computational Method

We perform the calculations by considering four different morphological types, dividing each type into 3 different luminosity classes (where the width of each class in absolute magnitude is 2), and allowing each of the luminosity classes for a specific type to form at 20 different discrete redshift intervals from $z = 0$ to $z = 2.5$, the relative proportion being determined by the distribution of formation times for galaxies of a specific luminosity (as discussed in §3). Then, for each of these $4 \times 3 \times 20 = 240$ distinct galaxy evolution histories, we determine how the gas, metallicity, star formation rate, and luminosity evolves. Finally, Monte Carlo catalogues are constructed using the quoted selection criteria, the given number densities, and these computed luminosity histories.

5. High Redshift Comparisons

As already mentioned, all our models have been constrained to reproduce the bulge-to-total distribution for the DJ and PB samples as can be seen in Figure 4. Comparisons with bulge $B - R$ colors and differences between bulge and disk $B - R$ colors are presented in Figure 5. Both our early bulge formation model and simultaneous bulge formation model produce good fits to the bulge colours and relative bulge-to-total colours at low redshift. Clearly, in the secular evolution model, not only are the bulges of local galaxies too blue relative to the disks, but there is more dispersion in both the bulge colours and bulge-to-disk relative colours than there is in low redshift samples. If necessary, inclusion of a small amount of reddening in the models would give better agreement with the low redshift data. It is also possible that the irregular morphology and/or potential AGN activity might cause these blue-bulged galaxies to be removed from the local samples.

We now examine the predictions of these different scenarios in terms of the higher redshift ($z \sim 1$) observations. Since the essential difference between the models is the formation time of bulges relative to the fiducial formation time of disks, we shall focus on the observables directly contrasting the bulge and disk properties: in particular, the high-redshift bulge-to-disk ratios and the high-redshift bulge-to-disk colours in our comparisons (see Figures 4-6). We begin by comparing our models to the bulge-to-total ratios of high redshift galaxies in the CFRS sample in Figure 4. We examine both the ground-based sample of Schade et al. (1996) and the HST-selected large disk ($r > 4h_{50}$ kpc) subsample of Lilly et al. (1998) in three different redshift intervals. To compare our models with the observations, we have generated Monte-Carlo catalogues of galaxies with bulge-to-total ratios in the observed $F814W$ band, applying the CFRS selection criteria ($I_{AB} < 22.5$ and a central I_{AB} surface brightness < 24.5) and the size cut ($h > 4$ kpc) to compare specifically with the Lilly et al. (1998) large disk subsample.

We subdivide the samples into the redshift bins (0.2,0.5), (0.5, 0.75), and (0.75, 1.00). While the differences between the models are quite small at low z, interesting differences begin to arise at $z \sim 1$. Unfortunately, at $z \sim 1$, the observed $F814W$ band is approximately probing rest-frame B light and hence is quite sensitive to active star formation. Consequently, the ordering of Models I, II, and III in terms of the number of galaxies with large B/T ratios is not the same as the order in which bulges form in these three models. The secular evolution model (Model I), with late bulge formation, has a paucity of large B/T objects relative to the other models. The simultaneous bulge formation model (Model II) has a large number of such galaxies simply because a large number of bulges were forming at this time, while the early bulge formation model (Model III) has a slightly lower value due to the fact that bulges in this model had long been in place within

their spiral hosts. Presumably, high resolution infrared images as will be available with NICMOS should be a more powerful discriminant between these models since it is more sensitive to total stellar mass than it is to current star formation. Unfortunately, both the lack of data and uncertainties in this data (± 0.2 in B/T) (Schade et al. 1996) are too large to permit any strong statements. It does appear, nevertheless, that there are too many large B/T systems observed (Lilly et al. 1998) relative to the models, and therefore there may be a lack of high B/T galaxies in our model of high luminosity, large disks.

We now look at the bulge colours and relative bulge-disk colours of high redshift galaxies. For our first sample (32 galaxies), for which HST images of CFRS-selected galaxies were available, we utilize the colours and bulge-to-total ratios compiled in Table 1 and Figure 5 of Schade et al. (1996). Following Schade et al. (1996) in the use of the best-fitting CWW SED templates for the purposes of k-corrections and colour conversions, we calculate the colours for the bulge-disk components from the total integrated $(U - V)_{0,AB}$ colours, the tabulated bulge-to-disk ratios given in the rest-frame B band, and the $(U - V)_{0,AB}$ colours of the indicated component. For our second sample (27 galaxies), we consider the bulge-to-disk colours compiled by Abraham et al. (1998) from a subsample of the Bouwens, Broadhurst, & Silk (1998a) sample, for which both $z > 0.3$ and fits to the bulge-to-total ratio were available (Ratnatunga et al. 1998). Note that the bulge (disk) colours compiled by Abraham et al. (1998) are determined from the light inside (outside) a 3-pixel aperture and are not determined from a proper bulge-disk decomposition. Using the best-fit CWW SED templates, we convert the Abraham et al. (1998) colours to their rest-frame values. We plot the data separately for these two samples due to potentially different systematics. Because of the larger uncertainties involved in determining the relative bulge-disk colours for galaxies dominated by a bulge ($B/T > 0.55$) or disk component ($B/T < 0.1$), we have excluded these galaxies from our comparisons due to the potentially large errors in the determination of the disk and bulge colours separately. For both data sets, we again compare with Monte-Carlo catalogues generated using the CFRS selection criteria due to its close similarity with the Bouwens et al. (1998a) selection criteria ($I_{F814W,AB} < 22.33$). We present histograms of the bulge colours and relative bulge-to-disk colours in Figure 5, and a scatter plot of the bulge-to-total ratios both versus the bulge colours and versus the relative bulge-to-disk colours in Figure 6. For both Figures 5-6, we subdivide the galaxies into the redshifts bins (0.3, 0.5), (0.5, 0.75), and (0.75, 1.0).

As expected, in all redshift bins, bulges are slightly bluer in the late bulge formation models than are the disks (Figure 5). A blue tail may be marginally detectable in the Schade *et al.* data in the highest redshift bins. Unfortunately, given the extremely limited amount of data and uncertainties therein, little can be said about the comparison of the models in all three redshift bins, except that the range of bulge and relative bulge-to-disk

colours found in the data appears to be consistent with that found in the models.

Figure 6 shows that the scatter in the data can readily be reproduced at both low and high redshift for the various models. Clearly, the secular evolution and other bulge formation models separate out in this diagram, late bulge formation models always yielding bluer bulges for a given B/T ratio. Unfortunately, the observational data set is sufficiently small and contains enough uncertainties (an estimated ± 0.1 in the B/T ratio and ± 0.3 in relative bulge-disk colours) that it is difficult to verify whether there is a paucity of blue bulges at high redshift relative to the predictions of the secular evolution model, though there appears to be several bluer bulges in the redshift interval (0.5,0.75).

6. Summary

We have developed three representative models for bulge formation and evolution. While consistent with currently available data, our models are schematic and are intended to illustrate the observable predictions that will eventually be made when improved data sets are available in the near future. Our models are (i) secular evolution, in which disks form first, (ii) simultaneous formation of bulge and disk, as might be expected in a monolithic model, and (iii) early bulge formation, in which bulges form first. We normalize to two local $z = 0$ samples which provide template bulge and disk luminosity ratios and colours. We make predictions for these bulge and disk parameters to $z \sim 1$ for comparison with observed samples.

Admittedly, our models are still quite crude, assuming among other things that the effects of number evolution on the present population of disks can be ignored to $z \sim 1$ as suggested, for example, in Lilly *et al.* 1998. Of course, one recent analysis (Mao, Mo, & White 1998) has argued that observations favor the interpretation that a non-negligible amount of merging has taken place in the disk population from $z = 0$ to $z = 1$. For this particular interpretation, it is not clear to us how all the present stellar mass in disks could have built up if disks were continually destroyed by merging to low z given the constraints on the cosmic star formation history.

We have also not considered the environmental dependencies that are sure to be important in the generation of the Hubble sequence. We plan on addressing these shortcomings in future work (Bouwens et al. 1998b) in the context of a semi-analytical hierarchical clustering model where we consider the formation of bulges by both secular and hierarchical evolution.

REFERENCES

Abraham, R.G., Ellis, R.S., Fabian, A.C., Tanvir, N.R., & Glazebrook, K. 1998, MNRAS, submitted.

Baugh, C.M., Cole, S. & Fremk, C.S. 1996, MNRAS, 283, 1361.

Binggeli, B., Sandage, A., & Tammann, G.A. 1988, ARA&A, 26, 509.

Bouwens, R.J., Broadhurst, T.J., & Silk, J. 1998a, ApJ, in press.

Bouwens, R.J., et al. 1998b, in preparation.

Buzzoni, et al. 1992, AJ, 103, 1814.

Calzetti, D. 1997, to appear in the Proceedings of the Conference "The Ultraviolet Universe at Low and High Redshift" preprint: astro-ph/9706121.

Connolly, A.J., Szalay, A.S., Dickinson, M., Subbarao, M.U., & Brunner, R.J. 1997, ApJ, 486, L11.

Courteau, S. 1996, to appear in "Morphology and Dust Content in Spiral Galaxies", Kluwer, Dordrecht, eds. D. Block & M. Greenberg.

de Jong, R.S. & van der Kruit, P.C. 1994, A&AS, 106, 451.

de Jong, R.S. 1995, A&AS, 118, 557.

de Jong, R.S. 1996, A&A, 313, 45.

Eggen, O., Lynden-Bell, D., & Sandage, A. 1962, ApJ, 136, 748.

Friedli, D., & Benz, W. 1995, A&A, 301, 649.

Gonzàlez, J.J. & Gorgas, J. 1996, ASP Conf. Ser., 86, 225.

Jablonka, P., Martin, P. & Arimoto, N. 1996, AJ, 112, 1415.

Kauffmann, G. & White, S.D.M. 1993, MNRAS, 261, 921.

Kormendy, J. 1992, in Proc IAU Symp.153, "Galactic Bulges", p. 209, Kluwer, Dordrecht, eds. Dejonghe, H. & Habing, H.

Lauberts, A., & Valentijn, E.A. 1989, The Surface Photometry Catalogue of the ESO Sky Survey (ESO, Garching).

Lacey, C. & Cole, S. 1993, MNRAS, 262, 627.

Leitherer et al. 1996, PASP, 108, 996.

Lilly, S.J., LeFevre, O., Hammer, F., & Crampton, D. 1996, ApJ, 460, L1.

Lilly, S.J., et al. 1998, ApJ, submitted.

Madau, P., Ferguson, H.C., Dickinson, M.E., Giavalisco, M., Steidel, C.C., & Fruchter, A. 1996, MNRAS283, 1388.

Mao, S., Mo, H.J., & White, S.D.M. 1998, ApJ, submitted, astro-ph/9712167.

McGaugh, S.S., & de Blok, W.J.G. 1997, ApJ, 481, 689.

Meurer, G.R., Heckman, T.M., Lehnert, M.D., Leitherer, C., & Lowenthal, J. 1997, AJ, 114, 54.

Molla, M. & Ferrini, F. 1995, ApJ, 454, 726.

Norman, C.A., Sellwood, J.A., & Hasan, H. 1996, ApJ, 462, 114.

Peletier, R.F., Valentijn, E.A., Moorwood, A.F.M., & Freudling, W. 1994, A&AS, 108, 621.

Peletier, R.F., Valentijn, E.A., Moorwood, A.F.M., Freudling, W, Knapen, J.H., & Beckman, J.E. 1995, A&AS, 300, L1.

Peletier, R.F. & Balcells, M. 1996, AJ, 111, 2238-2242.

Pfenniger, D. 1992, in Proc IAU Symp.153, "Galactic Bulges", p. 387, Kluwer, Dordrecht, eds. Dejonghe, H. & Habing, H.

Pozzetti, L., Bruzual, G., & Zamorani, G. 1996, MNRAS, 274, 832.

Ratnatunga, K.U., Griffiths, R.E., & Ostrander, E.J. 1998, in preparation.

Sawicki, M., & Yee, H.K.C. 1998, AJ, in press.

Schade, D., Lilly, S.J., Le Fevre, O., Hammer, F., & Crampton, D. 1996, ApJ, 464, 79.

Schade, D., Lilly, S.J., Crampton, D., Hammer, F., Le Fevre, O., & Tresse, L. 1995, ApJ, 451, L1.

Tinsley, B .M. 1980, Fund. Cosm. Phys., 5, 287.

White, S.D.M., & Frenk, C., 1991, ApJ, 379, 52.

Zaritsky, D., Kennicutt, R.C., & Huchra, J.P. 1994, ApJ, 420, 87.
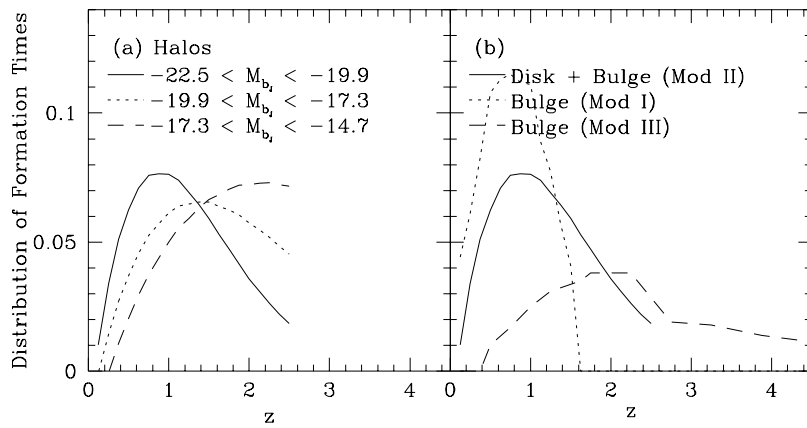
Fig. 1.— (a) Distribution of halo formation times for disk galaxies of different luminosities. (b) Distribution of disk and bulge formation times in Models I (secular evolution model), II (simultaneous formation model), and III (early bulge formation model).
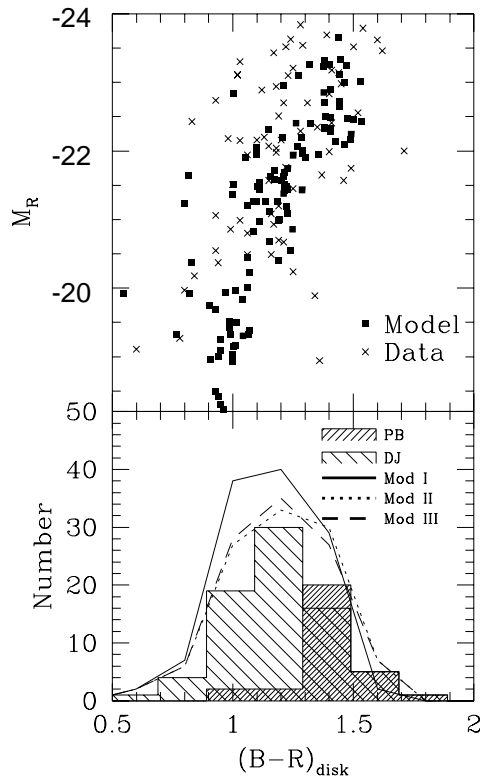
Fig. 2.— Comparison of local disk properties with our model predictions. The lower panel presents the $B - R$ colour distribution. Mod I (solid line) corresponds with the secular evolution model, Mod II (dotted line) corresponds with simultaneous formation model, and Mod III (short dashed line) corresponds with the early bulge formation model. The upper panel presents a scatter plot of the observed and predicted colour-magnitude relationship. For both panels, observational data are taken from Peletier & Balcells 1996 (dashed histogram) and de Jong 1995 (solid line histogram). Note that all the models use exactly the same disk model and thus give the same results, except for small differences observable in the figure due to our use of three different realizations.
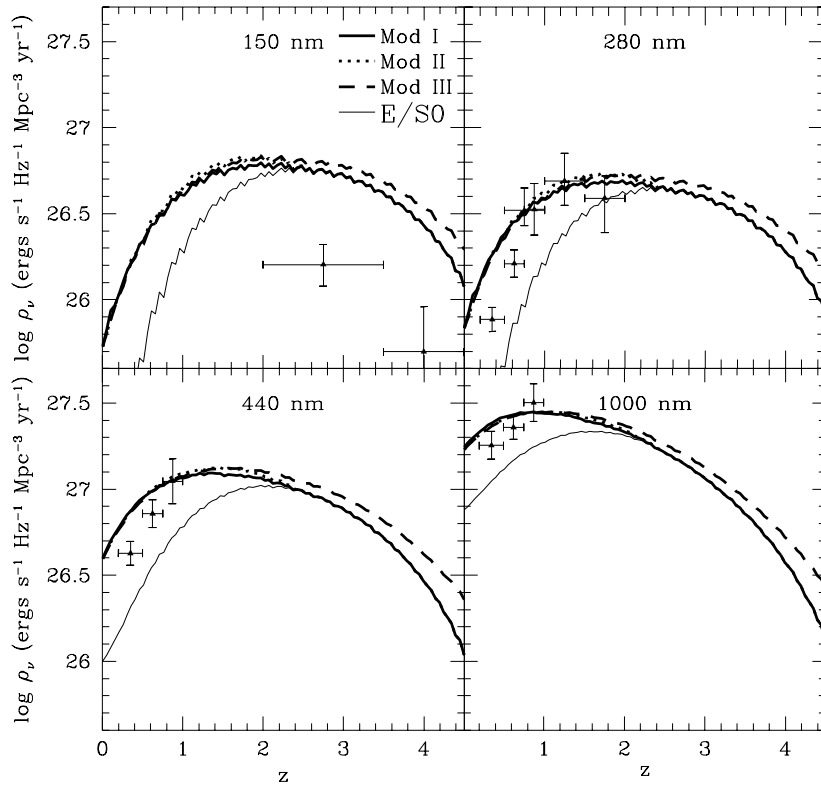
Fig. 3.— Comparison of the observed luminosity density at 150 nm, 280 nm, 440 nm, and 1000 nm against that predicted from our models including both the disk, bulge, and elliptical components. The contribution of E/S0 galaxies has been explicitly plotted to illustrate its contribution to the total. Observational data is taken from Madau et al. (1996) at 150 nm, Lilly et al. (1996) and Connolly et al. (1997) at 280 nm, Lilly et al. (1996) at 440 nm, and Lilly et al. (1996) at 1000 nm.
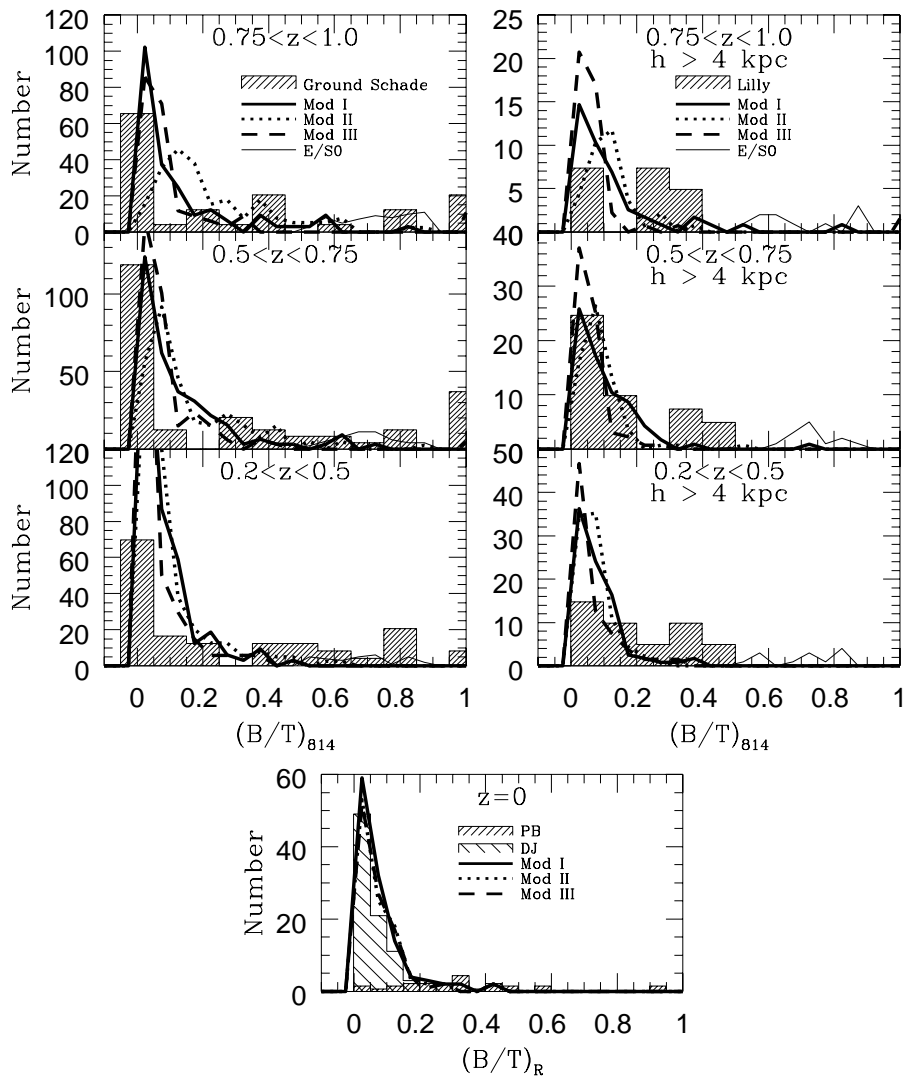
Fig. 4.— Comparison of the observed bulge-to-total ratios (histograms) with three different bulge formation models (see Figure 2 for a description) at both high and low redshift. High redshift comparisons are performed in the upper left panels against the Schade et al. (1996) data using the CFRS selection criteria and in the upper right panels against the Lilly et al. (1996) data using the CFRS selection criteria plus a size cut ($h > 4kpc$). $E/S0$ predictions are also included in the high redshift figures (long dashed line). Models are renormalized to match the data. Data used for the low-redshift comparisons are as in Figure 2.
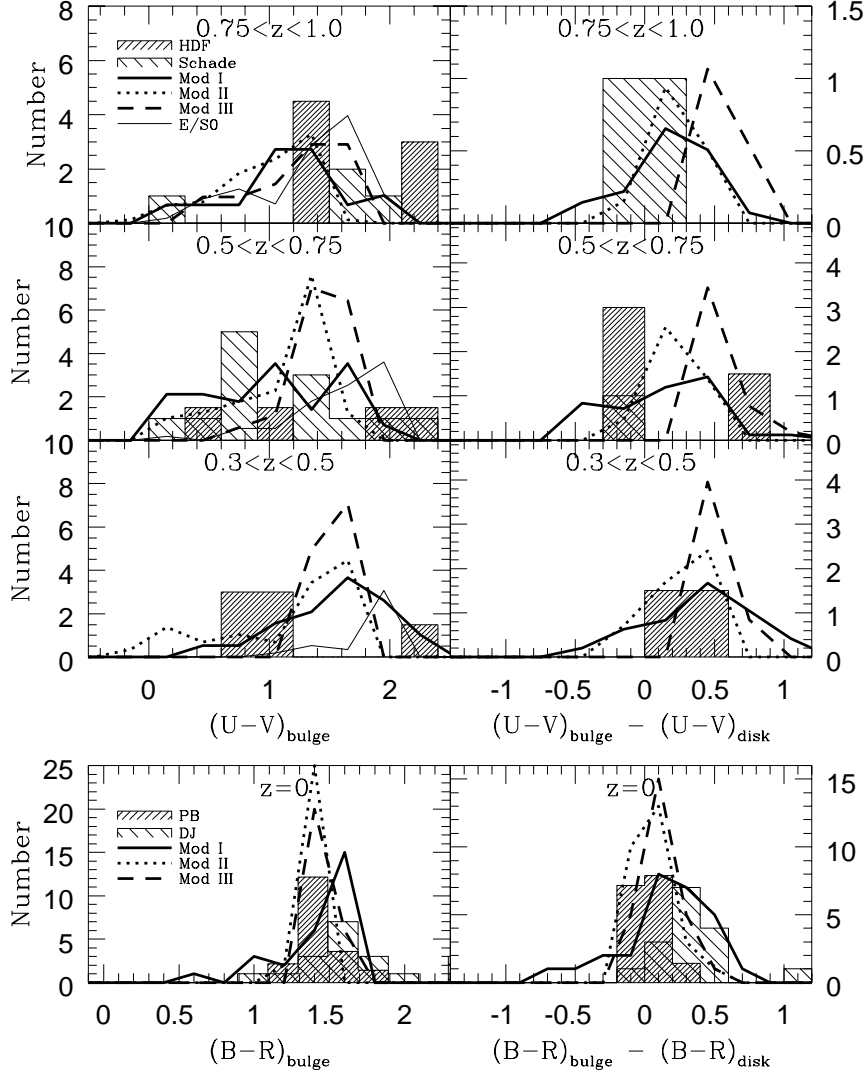
Fig. 5.— Comparison of the observed bulge and relative bulge-to-disk colours (histograms) with those of the models, at both high and low redshift. Model curves (renormalized to match observations and multiplied by 1.6 to increase their prominence) and low redshift data are represented as in Figure 4. The high redshift comparison includes data from the HDF for the Bouwens et al. (1998) sample (shaded histogram) and HST data from Schade et al. (1995) (open histogram).
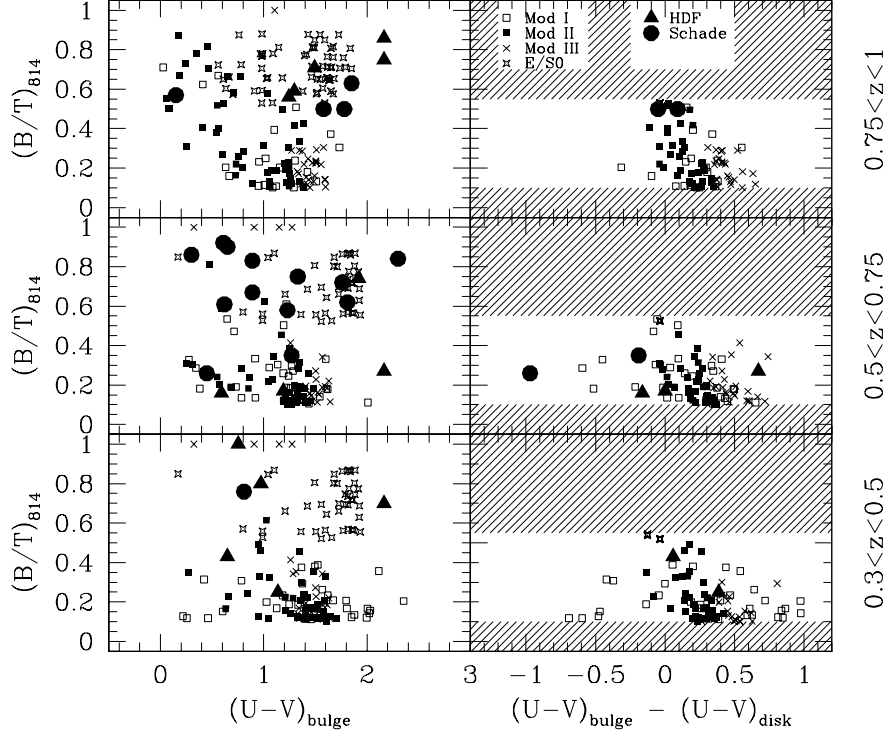
Fig. 6.— Observed bulge-total ratio vs. bulge and relative bulge-to-disk colours compared to Monte-Carlo realizations of these same quantities for our secular evolution model (open squares), our primordial collapse model (solid squares) and our early bulge formation model (crosses) as well as our E/S0 model (stars). The observational data are taken from the same two samples as in Figure 5, the Bouwens et al. (1998) HDF sample (solid triangles) and the Schade et al. (1996) sample (solid circles). The shaded areas in the right panels correspond to galaxies dominated by the bulge ($B/T > 0.55$) and by the disk ($B/T < 0.1$) excluded from the comparison for reasons that are explained in the text.